Journal of the Korean Physical Society, Vol. 69, No. 12, December 2016, pp. 1798∼1804

Characteristics of Resistive Switching in ZnO/SiO_x Multi-Layers for Transparent Nonvolatile Memory Devices

Kyongmin Kim
Department of Nano Engineering, University of Seoul, Seoul 02504, Korea

Eunkyeom Kim
DSM, Applied Materials Korea, Gyeonggi 18382, Korea

Youngill Kim
Convergence Research Center for Solar Energy, Daegu Gyeongbuk Institute of Science & Technology, Daegu 42988, Korea

Jung Hyun Sok and Kyoungwan Park*
Department of Physics, University of Seoul, Seoul 02504, Korea

(Received 24 October 2016)

Bipolar resistive switching in ZnO/SiO_x bi-layer and $ZnO/SiO_x/ZnO$ tri-layer structures was investigated for nonvolatile memory applications. ZnO thin films were grown using the radio-frequency magnetron sputtering technique at room temperature. SiO_x films were grown using plasma-enhanced chemical-vapor deposition at 200 °C. Multiple high-resistance states were observed during the set process. The high/low resistance state ratio was ∼10 during ∼100 on/off cycles. The tri-layer memory device exhibited better endurance properties than the bi-layer device. Because an asymmetric conducting filament has a weak point for charge conduction at the oxide interfaces, we attributed the good endurance property to the reproducible formation/rupture of "micro"-conducting filaments. Moreover, the dynamics of the oxygen ions in the SiO_x layer plays an important role in resistive switching.

PACS numbers: 73.21.Ac, 73.40.Sx, 81.05.Dz, 85.30.-z
Keywords: ZnO, Multilayer, Resistive switching, Nonvolatile memory, RRAM
DOI: 10.3938/jkps.69.1798

I. INTRODUCTION

Since the discovery of resistive switching in several binary transition-metal oxides, such as NiO, TiO_2, ZrO_2, HfO_2, and ZnO [1], the metal-oxide-based resistance random access memories (RRAM) have been widely considered as a future nonvolatile memory device owing to its simple and highly scalable memory structure, as well as its potentially high switching speed and low power consumption during memory operations [1]. Recently, resistive switching has also been observed in defective SiO_2 thin films, although silicon is not a binary transition metal [2–4]. Among the various metal oxides, ZnO has been demonstrated to be a RRAM candidate because it is not only abundant and environment-friendly raw material but also a material that is compatible with silicon technology [5–8]. Moreover, ZnO possesses a direct and wide bandgap of ∼3.4 eV. This material is highly transparent in the visible range; thus, a transparent ZnO-based RRAM device has been reported recently [9,10]. With respect to nonvolatile memory switching, thin ZnO films exhibited excellent resistive switching characteristics, including a fast switching speed [6], a large on/off resistance ratio [5], and long retention time [8]. Nevertheless, in many experiments, ZnO-based RRAM devices have demonstrated poor endurance during less than 100 on/off cycles [5,8], which can be attributed to the unstable and unrepeatable resistance states of this RRAM device.

Resistive switching arises when the oxide layer's resistance alternates between a high resistance state (HRS) and a low resistance state (LRS); these transitions can be controlled by applying an electric field. The conducting filament (CF) model, in which the formation/rupture of CFs consisting of oxygen vacancies changes the state of the oxide layer's resistance, is often used to explain the switching and/or conduction mechanisms [1]. However, this device is subject to increasing stress with increasing

*E-mail: kwpark@uos.ac.kr; Fax: +82-2-6490-5007

 ©2016 The Korean Physical Society

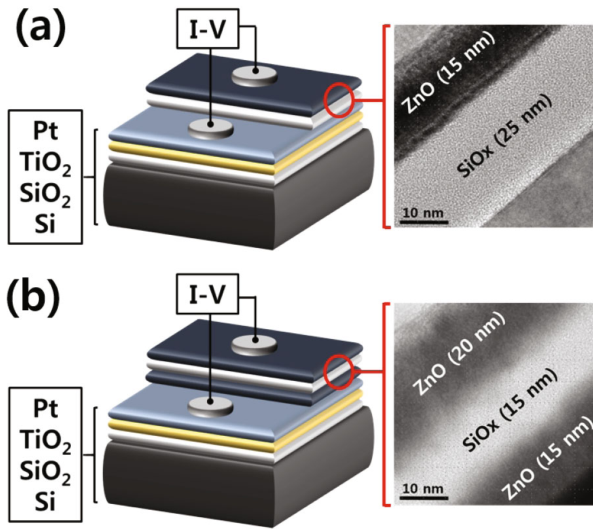

Fig. 1. (Color online) Schematics and cross-sectional TEM images of the (a) ZnO/SiO_x bi-layer device and the (b) ZnO/SiO_x/ZnO tri-layer device.

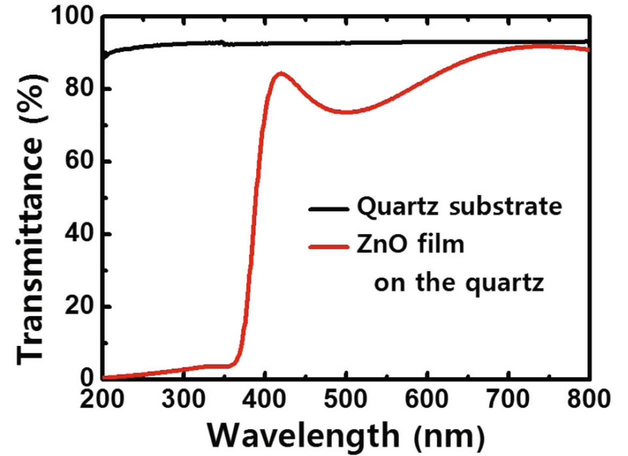

Fig. 2. (Color online) Optical transmission spectrum of the quartz substrate and of the ZnO layer on the quartz substrate.

number of on/off memory switching cycles. In addition, paths of CFs can randomly form in the oxide layer during the set process. Thus, the poor endurance of the ZnO-based RRAM is presently attributed mostly to the random formation of CF paths in the oxide layer.

On the other hand, CuO/ZnO and ZrO_x/HfO_y bilayers reportedly exhibit very good resistive switching properties [11, 12]. In particular, in the latter a high program/erase speed (40 ns) and significant endurance (10^7 cycles) were attributed to the minimal consumption of oxygen ions during on/off switching in a ZrO_x/HfO_y bilayer RRAM device [12]. An asymmetric CF, narrowing at the ZrO_x/HfO_y interface, was suggested to have formed in this device. The CF formation and rupture sites were confined to the ZrO_x/HfO_y interface, and oxygen consumption during switching was suppressed. In this study, ZnO/SiO_x bi-layer and ZnO/SiO_x/ZnO tri-layer films sandwiched between Al and Pt electrodes were fabricated for nonvolatile ZnO-based RRAM applications to increase the devices' endurances. Typical bipolar resistive switching characteristics were demonstrated. Formation/rupture of "micro"-conducting filament paths at the ZnO/SiO_x interfaces was expected to improve the endurance of resistance fluctuations in the HRS and the LRS. In addition, switching was accomplished using a very small bias current because SiO_x is a well-known and robust insulator.

II. EXPERIMENTAL DETAILS

Thin SiO_x ($x < 2$) and ZnO layers were prepared using plasma-enhanced chemical-vapor deposition (PECVD) and radio-frequency magnetron-sputtering techniques, respectively. To fabricate the ZnO/SiO_x bi-layer structure, we deposited 25-nm-thick SiO_x films on substrates in the presence of SiH_4 (5 % diluted in He) and N_2O gases at 200 °C. The substrate consisted of Pt/TiO_2/SiO_2 layers on a silicon wafer. ZnO thin films (thickness: 15 nm) were successively deposited on the SiO_x layer by using a ZnO target (diameter: 2 inch, purity: 99.999 %) at room temperature. Sputtering was performed in the presence of an Ar ambient at a pressure of 5 mTorr. The top 300-nm-thick electrodes (Al: 99.999 %) were deposited using a metal shadow mask in a vacuum evaporation system. Positive and negative voltages were applied to the Al top electrode (diameter: 300 μm) during the current-voltage (I-V) measurements while the Pt bottom electrode was grounded.

To fabricate the ZnO/SiO_x/ZnO tri-layer structure, we deposited a 15-nm-thick ZnO film on the substrate by using the sputtering method. Then, a SiO_x film (thickness: 15 nm) was deposited on the ZnO layer by using the PECVD technique. The second ZnO thin film (thickness: 20 nm) was formed on the SiO_x/ZnO/Pt layer under the same conditions as those used with the previous sputtering deposition. The electrode fabrication was similar to the previous one. To analyze the properties of the ZnO and the SiO_x films, we utilized transmission electron microscopy (TEM), visible transmission spectroscopy, X-ray diffraction (XRD), and X-ray photoelectron spectroscopy (XPS). Measurements of the resistive switching characteristics were performed using an Agilent 4155C LCR Meter in a dark environment. Figure 1 shows schematics and cross-sectional TEM images of the fabricated ZnO-based RRAM devices.

III. RESULTS AND DISCUSSION

Figure 2 shows the optical transmission characteristics of the ZnO layer deposited on a quartz substrate. The

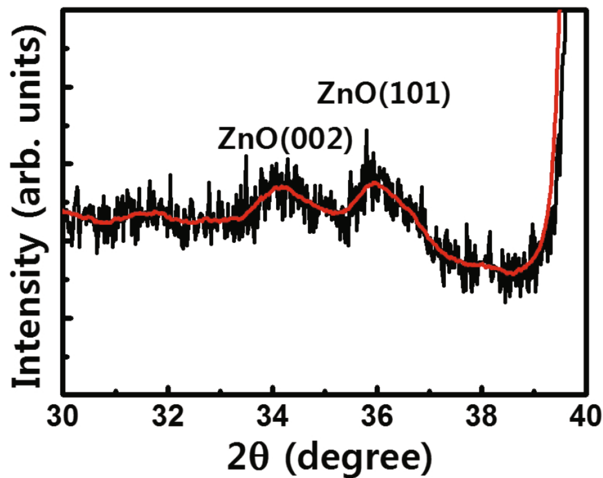

Fig. 3. (Color online) XRD spectrum of the ZnO film deposited on the Pt/Ti/SiO_2/Si substrate at room temperature.

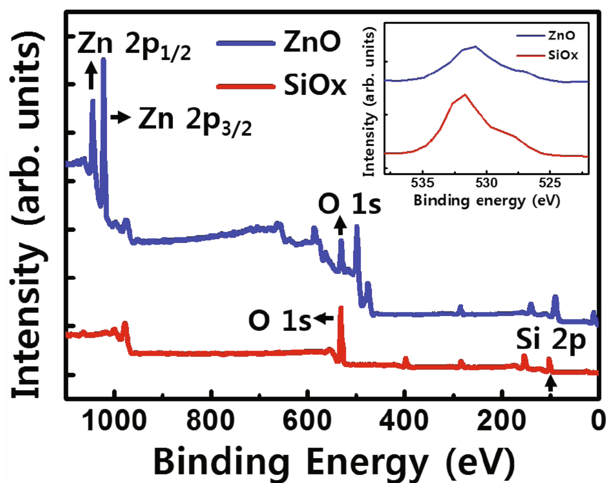

Fig. 4. (Color online) XPS spectra of the ZnO film on the SiO_x layer and of the SiO_x film on the Pt/Ti/SiO_2/Si substrate. The inset shows the O 1s XPS spectra.

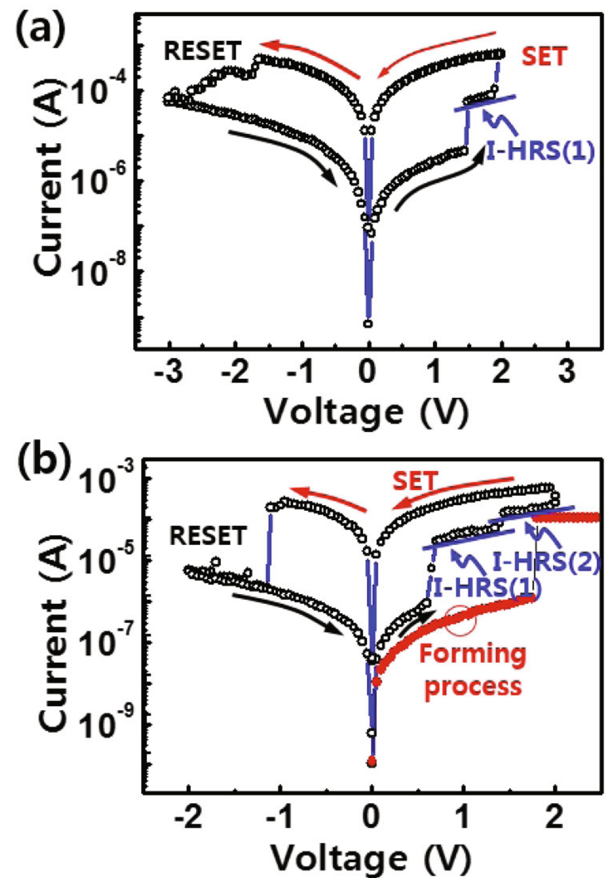

Fig. 5. (Color online) Bipolar resistive switching characteristics of the (a) ZnO/SiO_x bi-layer device and the (b) ZnO/SiO_x/ZnO tri-layer device.

transmittance of the ZnO layer was in the 70 % - 80 % range in the visible region. These results justify the use of the fabricated ZnO thin films as transparent memory devices. The XRD spectrum for the ZnO thin film deposited on the Pt/Ti/SiO_2/Si substrate is shown in Fig. 3. The spectrum contains several diffraction peaks, 34.2° and 36.0°, which correspond, respectively, to the (002) and the (101) planes of hexagonal ZnO wurtzite [8, 9]. The broad low-intensity peaks indicate that the ZnO film has moderate crystallinity and a polycrystalline-like structure.

The XPS spectrum of the ZnO layer on the SiO_x layer and the spectrum of the SiO_x layer are presented in Fig. 4. For the ZnO layer, two peaks, one each at binding energies of 1021.2 eV and 1044.2 eV, are observed, which correspond to the $2p_{3/2}$ and $2p_{1/2}$ spin-orbit coupling states of Zn, respectively. The binding energy difference (23.0 eV) between these peaks suggests that most Zn atoms in the sputtering-deposited ZnO film are in the fully oxidized state (Zn^{2+}) and that the film does not contain metallic Zn atoms [5]. The peak with a 530.9 eV binding energy, which is related to the O 1s level, can be decomposed into two peaks; one peak (530.3 ± 0.2 eV) is attributed to O^{2-} ions chemically bonded to Zn^{2+} ions in the wurtzite structure of crystalline ZnO while the other (531.6 ± 0.3 eV) is associated with O^{2-} ions in oxygen-deficient regions within the ZnO matrix [6, 13]. The Si 2p and O 1s peaks appear at binding energies of 103.0 eV and 530.9 eV, respectively, in the SiO_x layer. Compared with the previous XPS results for stoichiometric SiO_2 thin films, the PECVD-grown SiO_x layer in this work is thought to be nonstoichiometric and oxygen-atom-deficient [3,14]. The inset of Fig. 4 shows that the intensity of the high-binding-energy side of the O 1s peak is higher for the ZnO layer than for the SiO_x layer (the full width at half maximum of the ZnO O 1s peak is larger than that of the SiO_x O 1s peak). Therefore, we speculate that the ZnO layer may possess more oxygen vacancies than the SiO_x layer.

Figure 5 shows representative *I*-*V* characteristics of

the ZnO/SiO$_x$ bi-layer and the ZnO/SiO$_x$/ZnO tri-layer devices. After a positive-voltage electro-forming process, the ZnO/SiO$_x$ bi-layer device exhibited bipolar resistive switching when a DC voltage was swept in a $0 \rightarrow +2 \rightarrow 0 \rightarrow -3 \rightarrow 0$ V sequence. When the positive voltage was applied to the top electrode, a sudden increase in the current was observed at 1.5 V. This phenomenon is known as an "intermediate" set process, during which the device switches from the HRS to an intermediate HRS. Through an additional set process, clearly observed at 1.9 V, the device switched from the intermediate HRS to the LRS. The LRS was maintained as the applied voltage was swept from +2 V to 0 V. When the bias voltage was swept in the negative direction, a gradual reduction in the current was observed for voltages above −1.6 V owing to a resistance change in the device; the device switched from the LRS to the HRS in a reset process. The HRS was maintained as the applied voltage was swept from −3 V to 0 V. On the other hand, the ZnO/SiO$_x$/ZnO tri-layer device exhibited intermediate set processes at 0.6 V and 1.3 V, and the LRS was obtained at 2.0 V as the voltage was swept in the positive direction ($0 \rightarrow +2$ V). A sharp reset process appeared at −1.1 V during the negative voltage sweep ($0 \rightarrow -2$ V). In between the set and the reset voltages, the device maintained its resistance state. Before the set/reset *I-V* characteristics had been measured, an electro-forming process took place at ∼1.8 V under current compliance (0.1 mA) during the positive voltage sweep. The high/low resistance state current ratio was above 10^2.

Many RRAM devices were reported to be capable of multilevel memory operation [1, 15, 16]. In a TiN/TiO$_x$/HfO$_y$/TiN RRAM device, three levels of the HRS resistance were shown for three different reset stop voltages, and three levels of the LRS resistance were obtained by changing the set current compliance [15]. Modulations of the ruptured CF length and of the CF diameter (or number) were suggested to underlie the emergence of multiple levels of the HRS and the LRS resistance, respectively. In this work, however, the number of HRSs corresponded to the number of different oxide layers between the device's electrodes. Therefore, we speculated that the complete set process of the device consisted of the individual set processes for the different constituent oxide layers. A CF was first formed in one oxide layer in the intermediate set process; then, a stronger electric field in the other oxide layer was created between the ends of pre-formed CFs at the interfaces between the oxide layers and the metal electrode. The higher voltage applied above the intermediate set voltage yielded a second formation of CFs in the other oxide layer (Fig. 5(a)). The set process was completed after these two CF formations. This picture can also explain the emergence of a three-level HRS via the formation of three CFs in the tri-layer RRAM device (Fig. 5(b)). Note that for the negative voltage sweep, the reset process of the tri-layer RRAM device is more pronounced than that of the bi-layer RRAM device.

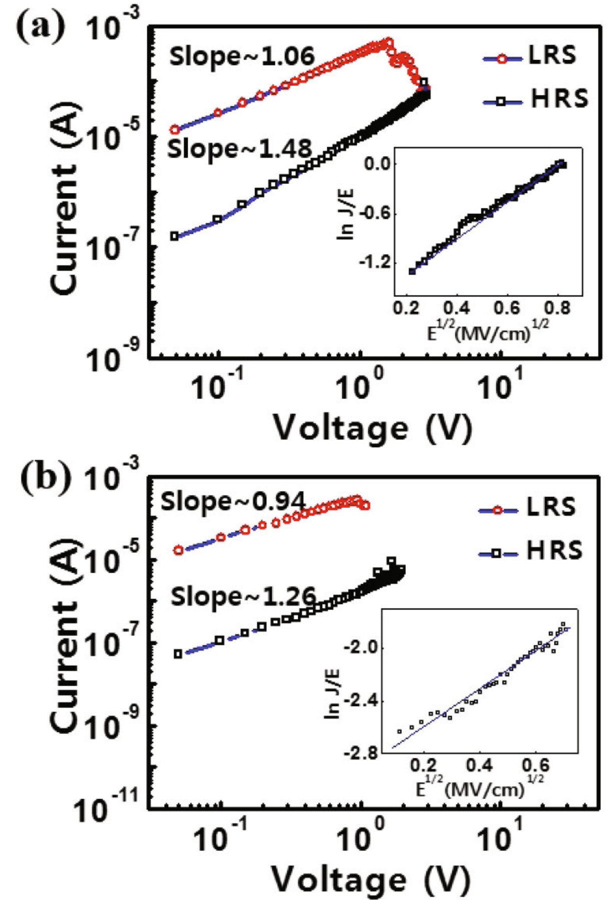

Fig. 6. (Color online) Current fits for the carrier transportation analysis of the (a) ZnO/SiO$_x$ bi-layer device and the (b) ZnO/SiO$_x$/ZnO tri-layer device. The insets show plots of $\ln(J/E)$ vs. $E^{1/2}$ in the HRS.

Resistive switching in a ZnO-based RRAM is attributed to the formation and the rupture of oxygen-vacancy conducting filaments with the dynamics of non-lattice oxygen ions [1,5,7–10]. When CFs are formed in the LRS, thermally-generated free electrons flow along the CFs driven by the bias voltage. Thus, most *I-V* plots of the LRS in ZnO RRAMs exhibit Ohmic behavior. However, the charge transport mechanism in the HRS depends on the presence of various defects, such as oxygen vacancies, metallic defects, dislocations, and grain boundaries in the ZnO matrix layer, that are considered after disconnecting the filaments. Owing to these defects, the nonlinear *I-V* behavior in the HRS was attributed to Poole-Frenkel (P-F) emission [5,9] or space-charge-limited current [7, 8, 10]. The charge transport mechanism in the SiO$_2$ layer depends on the electrode material. For example, Cu-metallic conduction and hopping transport were reported in the LRS and the HRS of a Cu/SiO$_2$/Au RRAM, respectively [3]. Bias-polarity-dependent resistance switching was also reported for a

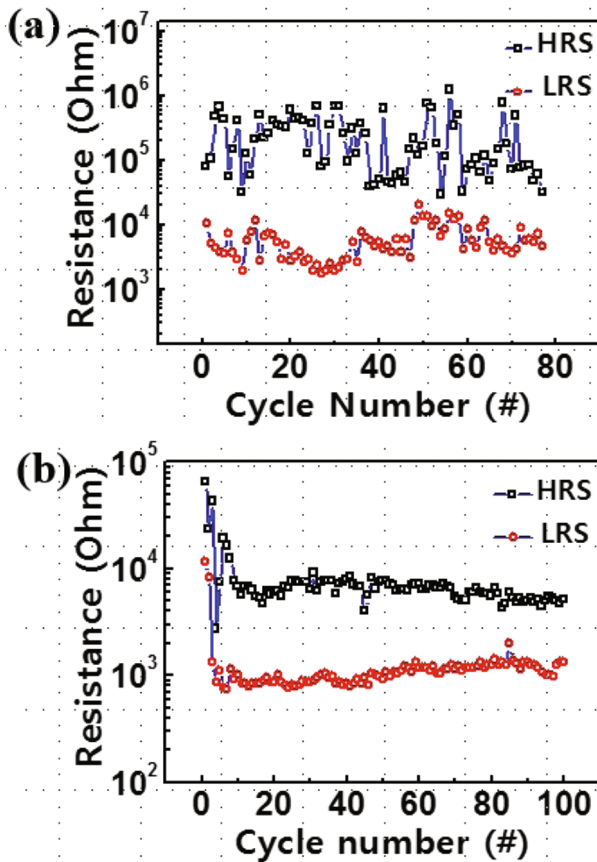

Fig. 7. (Color online) Endurance properties of the (a) ZnO/SiO_x bi-layer device and the (b) $ZnO/SiO_x/ZnO$ tri-layer device.

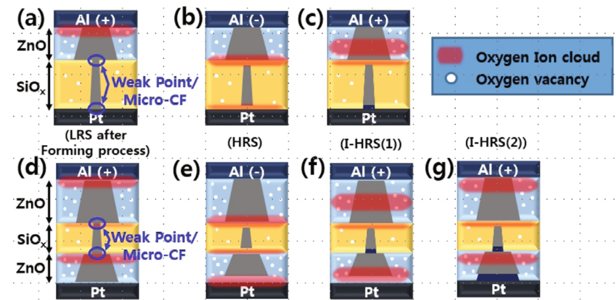

Fig. 8. (Color online) Schematics of the dependences of the proposed formation/rupture of "micro"-conducting filaments on the set/reset cycles for the (a) ZnO/SiO_x bi-layer device and the (b) $ZnO/SiO_x/ZnO$ tri-layer device.

$W/SiO_2/Pt$ RRAM device; the memory device exhibited typical electronic switching by initial electroforming with a negative bias voltage to the W electrode while ionic-defect-mediated (conducting filament) resistance switching was observed for the opposite-bias electroforming [4].

To analyze the charge transport mechanism, we replotted typical *I-V* curves (Fig. 5) on a double logarithmic axis, and various charge transport models were used for fitting the data. As shown in Fig. 6, the LRS demonstrated Ohmic conduction in both devices because the slope was ~1. However, the HRSs did not exhibit Ohmic conduction because in both cases, the slopes were above 1. According to the P-F emission mechanism, the *J-E* relation can be expressed as $J \propto E \cdot \exp(E^{1/2})$, where J is the current density and E is the applied electric field. Because the insets of Fig. 6 indicate that $\ln(I/E)$ is linear in $E^{1/2}$, these results for the HRSs in both devices can be well explained by using P-F emission. Because many types of defects are usually present in the ZnO and the SiO_x layers, the HRS conduction mechanism can possibly be attributed to P-F emission. We should note that although the RRAM devices in this work consisted of two or three different oxide layers (ZnO and SiO_2), the overall transport mechanisms are consistent with the CF model predictions of resistive switching.

The endurance characteristics of these devices are shown in Fig. 7. For the bi-layer and the tri-layer devices, the resistances during the endurance cycles were measured at +0.1 V and +0.25 V, respectively. During the resistive switching cycles, the average HRS-to-LRS resistance ratio was maintained at $\sim 10^{1.5}$ for the ZnO/SiO_x device and at $\sim 10^1$ for the $ZnO/SiO_x/ZnO$ device. However, fluctuation in the HRS and the LRS resistances were much smaller for the $ZnO/SiO_x/ZnO$ device than for the ZnO/SiO_x device.

In the CF model, the dynamics of oxygen vacancies and oxygen ions (O^{2-}) in the metal-oxide layers play an important role in the formation/rupture of CFs. In addition, the heterostructure and its interface have been shown to improve the bipolar resistive-switching behaviors in multi-oxide-layered structures [11,12]. Here, we propose a mechanism of the formation/rupture of micro-CFs in the bi-layer and the tri-layer RRAM structures based on the aforementioned CF model, which is shown in Fig. 8. In this model, initial electroforming is achieved by applying a positive voltage bias. Then, defects (oxygen vacancies) are generated and form CFs in both oxide layers. Thus, the device switches from the initial HRS to the LRS owing to the formation of complete CFs. Moreover, the physical size of a CF in an oxygen-vacancy-rich layer is larger than that of a CF in an oxygen-vacancy-deficient layer [12,17], such that the CF size in the ZnO layer is larger than the CF size in the SiO_x layer. Because oxygen ions move towards the top electrode owing to the positive voltage bias during the electro-forming process, the CFs formed in the oxide layers are trapezoid-shaped. Therefore, an asymmetric CF is formed, connecting the top and bottom electrodes, as shown in Figs. 8(a, d). When charge is conducted through a conducting path, this asymmetric CF has weak points at the oxide interfaces. These weak points in the SiO_x layer are called microfilaments and are located at the two ends of the CF.

During the reset process (by applying a negative voltage bias), nonlattice oxygen ions in the ZnO layer move

into the SiO_x layer. In addition, the current flowing through the asymmetric CF causes a local Joule heating at the weak points. Consequently, the migrant oxygen ions associated with this local heating will easily oxidize the oxygen vacancies of the microfilaments, rupturing the microfilaments. The upper microfilament can be easily oxidized because the concentration of migrant oxygen ions is high at the ZnO/SiO_x interface. However, because of the ZnO/SiO_x interface barrier that prevents the migration of oxygen ions down to the Pt electrode, the lower microfilament is rarely oxidized, which leads to a slow reset process during the negative voltage sweep (Fig. 5(a)). A cross-sectional schematic of ruptured CFs, obtained after the reset process (during which the resistance state of the device changes from the LRS to the HRS), is shown in Fig. 8(b).

When a small positive voltage is applied during the set process, first a reduction reaction (generation of oxygen vacancies) occurs at the position of the lower microfilament of the SiO_x layer to form the lower microfilament because the electric field is higher in the SiO_x layer than in the ZnO layer and because oxygen ions accumulate near the ZnO/SiO_x interface so that the oxygen ions hinder the formation of an upper microfilament. Figure 8(c) shows the formation of the intermediate HRS(1) (I-HRS(1)) during the set process (also, see Fig. 5(a)). In addition, oxygen ions that escape owing to the generation of oxygen vacancies migrate back to the ZnO layer to re-form the CF by oxidizing a fraction of the oxygen vacancies. However, the CF in the ZnO layer is large enough, so the oxygen-ion's movement rarely influences the CF-rupture in the layer [12]. Under a large positive voltage, the oxygen ions that accumulate near the ZnO/SiO_x interface eventually overcome the interface barrier and migrate towards the top electrode, yielding a reduction process near the upper microfilament position to re-obtain the upper microfilament. As a result, the device switches back to the LRS, as shown in Fig. 8(a). However, the bi-layer device still exhibits large resistance fluctuations during endurance cycles owing to the nonreproducible formation of microfilaments.

In the tri-layer device, some oxygen ions are at the upper ZnO/SiO_x interface in the LRS because oxygen ions can be supplied from the bottom ZnO layer to the SiO_x layer during the positive-voltage electro-forming; the existence of these oxygen ions is somewhat different from that in the bi-layer device. During the negative voltage reset process, these oxygen ions at the upper ZnO/SiO_x interface migrate towards the lower SiO_x/ZnO interface to oxidize the oxygen vacancies (to rupture the lower microfilament) in local Joule heating. At the same time, the oxygen ions in the top and the bottom ZnO layers move down to the upper ZnO/SiO_x interface and Pt electrode and break the upper microfilament and the lower part of the CF formed in the bottom ZnO layer, respectively. We believe that this reset process is so fast that the device is sharply switched off in the negative range of voltages (Fig. 5(b)). Figure 8(e) schematically shows the filament configuration of the HRS.

The CF configurations of the two intermediate HRSs are shown in Figs. 8(f) and (g). During the set process with a small positive bias voltage, a reduction reaction first occurs in the lower microfilament position of the middle SiO_x layer to form the lower microfilament; this process is similar to that in the bi-layer device, as shown in Fig. 8(f). Under an intermediate-magnitude positive voltage, a regular CF is formed at the bottom of the ZnO/Pt electrode owing to the significant migration of oxygen ions towards the lower SiO_x/ZnO interface (Fig. 8(g)). When a high voltage is applied, oxygen ions accumulate near the ZnO/SiO_x interface, eventually overcoming the interface barrier and migrating towards the top electrode, yielding a reduction near the upper microfilament to re-obtain the upper microfilament. Then, the device switches back to the LRS, as shown in Fig. 8(d). This successive microfilament formation can be used to explain the emergences of the multiple HRS levels shown in Fig. 5(b). Therefore, the formation and the rupture of CFs relevant to resistive switching are limited to a very narrow region at the upper ZnO/SiO_x and SiO_x/lower ZnO interfaces. The tri-layer device exhibits smaller resistance fluctuations during endurance cycles than the bi-layer device owing to the reproducible formation of microfilaments in the SiO_x layer.

IV. SUMMARY

We investigated the resistive switching characteristics of RRAM devices with ZnO/SiO_x and ZnO/SiO_x/ZnO multilayer structures fabricated on Pt substrates. Both RRAM devices exhibited bipolar resistive switching with multiple high-resistance states. The dominant electrical transport modes in the LRS and the HRS in both devices were Ohmic conduction and P-F emission, respectively. The HRS/LRS resistance ratio for the tri-layer device was smaller than that for the bi-layer device, but the endurance of the tri-layer device was better than that of the bi-layer device over $\sim$100 endurance cycles. An asymmetric conducting filament is expected to possess weak points (microconducting filaments) for charge conduction that are confined to the oxide interfaces. The emergence of the multiple high-resistance states observed during the set processes and the better endurance of the tri-layer device can be explained in terms of the formation/rupture of microconducting filaments in the SiO_x layer, which are induced by the dynamics of oxygen ions driven by the bias voltage.

ACKNOWLEDGMENTS

This work was supported by the 2014 Research Fund of the University of Seoul.

REFERENCES

[1] H. S. P. Wong, H. Y. Lee, S. Yu, Y. S. Chen, Y. Wu, P. S. Chen, B. Lee, F. T. Chen and M. J. Tsai, Proceedings of the IEEE **100**, 1951 (2012), and many of the references are in this review paper.
[2] A. Mehonic, S. Cueff, M. Wojdak, S. Hudziak, O. Jambois, C. Labbé, B. Garrido, R. Rizk and A. J. Kenyon, J. Appl. Phys. **111**, 074507 (2012).
[3] S. Otsuka, T. Kato, T. Kyomi, Y. Hamda, Y. Tada, T. Shimizu and S. Shingubara, Jpn. J. Appl. Phys. **52**, 06GF04 (2013).
[4] H. Jiang, X. Y. Li, R. Chen, X. L. Shao, J. H. Yoon, X. Hu, C. S. Hwang and J. Zhao, Sci. Rep. **6**, 22216 (2016).
[5] W. Y. Chang, Y. C. Lai, T. B. Wu, S. F. Wang, F. Chen and M. J. Tsai, Appl. Phys. Lett. **92**, 022110 (2008).
[6] N. Xu, L. Liu, X. Sun, X. Liu, D. Han, Y. Wang, R. Han, J. Kang and B. Yu, Appl. Phys. Lett. **92**, 232112 (2008).
[7] C. Chen, F. Pan, Z. S. Wang, J. Yang and F. Zeng, J. Appl. Phys. **111**, 013702 (2012).
[8] J. Zhang, H. Yang, Q. I. Zhang, S. Dong and J. L. Luo, Appl. Phys. Lett. **102**, 012113 (2013).
[9] J. W. Seo, J. W. Park, K. S. Lim, J. H. Yang and S. J. Kang, Appl. Phys. Lett. **93**, 223505 (2008).
[10] F. M. Simanjuntak, D. Panda, T. L. Tsai. C. A. Lin, K. H. Wei and T. Y. Tseng, J. Mater. Sci. **50**, 6961 (2015).
[11] F. Yang, M. Wei and H. Deng, J. Appl. Phys **114**, 134502 (2013).
[12] C. Y. Huang, C. Y. Huang, T. L. Tsai, C. A. Lin and T. Y. Tseng, Appl. Phys. Lett. **104**, 062901 (2014).
[13] M. Chen, X. Wang, Y. H. Yu, Z. L. Pei, X. D. Bai, C. Sun, R. F. Huang and L. S. Wen, Appl. Surf. Sci. **158**, 134 (2000).
[14] Y. N. Sun, A. Feldman and E. N. Farabaugh, Thin Solid Films **157**, 351 (1988).
[15] H. Y. Lee, P. S. Chen, T. Y. Wu, Y. S. Chen, C. C. Wang, P. J. Tzeng, C. H. Lin, F. Chen, C. H. Lien and M. J. Tsai, *Tech. Dig. IEEE Int. Electron Devices Meeting* (2008), p. 297.
[16] W. K. Hsieh, K. T. Lam and S. J. Chang, Mat. Sci. Semicon. Proc. **35**, 30 (2015).
[17] M. H. Lin, M. C. Wu, C. Y. Huang, C. H. Lin and T. Y. Tseng, J. Phys.D: Appl. Phys. **43**, 295404 (2010).